Supplementary files for:

Reconfigurable Multistate MRAM Synapses with Vortex STNO based Neurons for Scalable In-Memory Convolutional Neural Networks

Ravish Kumar Raj[1,3,5], Simon N. Richter[3], Saeed Baghaee Ivriq[2], Oliver Fridorf[3], Darío Fernández-Khatiboun[1], Yasser Rezaeiyan[1], Sonal Shreya[3], Luana Benetti[4], Tim Boehnert[4], Ricardo Ferreira[4], Hooman Farkhani[1], Sonal Shreya[3] and Farshad Moradi[1, 3]*

[1]The Faculty of Engineering, Institute of Mechanical and Electrical Engineering Department, IME, University of Southern Denmark, Odense
[2]Electronic Circuits and Systems, KU Leuven, Arenberg Campus, Kasteelpark Arenberg, Belgium
[3]Department of Electrical and Computer Engineering, Aarhus University, Aarhus, Aarhus N 8200, Denmark
[4]International Iberian Nanotechnology Laboratory (INL), Braga, Portugal
[5]Department of Electronics and Communication Engineering, Indian Institute of Technology, Roorkee, India 247667
*Email: moradi@sdu.dk

1. Device characterization with on-chip (internal) field line

1.1. Measurement setup and methods

Measurement setup: The device was characterized using a manual probe station equipped with DC probes. Electrical biasing and readout were performed using source-meter units (SMUs), while dynamic and RF signals were monitored using a spectrum analyzer connected through a bias-Tee. All instruments were computer (PC)-controlled via a Python-based measurement program, enabling automated field line sweeps and synchronized data acquisition.

Figure S1 illustrates the complete experimental setup and measurement methods used for the electrical and RF characterization of the single array sample of 8 MRAM and 1 STNO device.

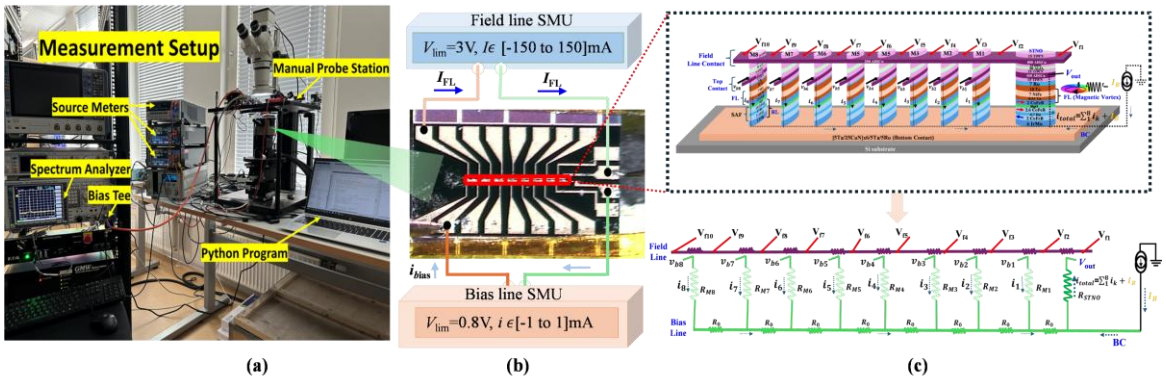

Figure S1: Experimental characterization setup and measurement methodology. (a) shows the laboratory setup comprising a manual probe station, source-meter units (SMUs), bias-tee, spectrum analyzer, and a Python-controlled data acquisition system (PC). (b) illustrates the probing configuration and electrical biasing scheme, where the field line is driven by one SMU and the bias line is driven by another one. (c) presents the device structure and layout, showing multiple MTJs connected along a common bottom contact on a Si substrate, together with the corresponding equivalent circuit used for weighted synapse and STNO as neuron.

MRAM characterization: As shown in Figure S1 (a), the sample is mounted on the probe-station chuck using thin double-sided tape and contacted using a manual probe station. Four probe terminals are employed: two probes are connected to the field line (FL) and two to the bias line (BL) of the device. A single-array sample fabricated at INL is used for the present measurements. An optical microscope integrated with the probe station is used to accurately align the probes with the device contact pads; the microscope image is streamed to the control computer via OBS. Care is taken to retract the microscope from the probing area before moving the sample to avoid mechanical damage. The magnetic field is generated by driving a current through the field line using an R&S source-measure unit (SMU), thereby controlling the field's strength via the applied current. Electrical biasing of the device is provided by a Keithley 2450 SMU, which is also used to measure the device's resistance to verify proper probe contact.

- **Field line (FL**): Driven by an SMU with a voltage compliance of $V_{\text{lim}} = 2$ V and current range $I_{\text{FL}} \in [-150, +150]$ mA. This line generates the magnetic field required for device switching.
- **Bias line (BL):** Driven by a separate SMU with a voltage compliance of $V_{\text{lim}} = 0.8$ V and current range $i_{\text{bias}} \in [-1, +1]$ mA, used to bias the magnetic tunnel junctions and reading the resistance state.

STNO characterization: For spin-torque nano-oscillator (STNO) measurements, a bias-tee (Figure S1) is used to separate the DC biasing and RF signal paths. The DC current from Keithley SMU is applied to the device through the bias-tee, while the generated RF oscillations are routed to an R&S spectrum analyzer. The spectrum analyzer is used to measure the output power spectral density of the device, with key parameters including frequency span, resolution bandwidth (RBW), and the number of capture points. These parameters are optimized to improve frequency resolution and reduce the noise floor, at the expense of increased acquisition time. Resistance measurements using the Keithley SMU are performed prior to RF measurements to ensure reliable electrical contact.

- **Field line (FL**): Driven by an SMU with a voltage compliance of $V_{\text{lim}} = 3$ V and current range $I_{\text{FL}} \in [-150, +150]$ mA. This line generates the magnetic field required for device switching.
- **Bias line (BL):** Driven by a separate SMU with a voltage compliance of $V_{\text{lim}} = 1$ V and current range $i_{\text{bias}} \in [-5, +5]$ mA, used to bias the magnetic tunnel junctions and reading the resistance state.

Device architecture and probing: Microscopy image of fabricated device that comprises of 8 in-plane elliptical MTJ having dimension (0.1µm x0.5µm) and 1 STNO with circular dimension of 0.35µm x 0.35µm on single array having common and individual field line controlled by Vf1, Vf2, ..Vf10 on top (dotted blue box) for writing path and weighted inputs (bias) from top contact vb1, vb2 …vb8 (dotted green box) to shared bottom contact (BC) pads for reading the states MRAM as a synapse. The MTJ cells are spaced 120 µm apart mostly due to the layout of the contacts pads and to eliminate stray field interactions between the neighboring MTJs. The complete material stack used in the devices investigated in this study consists of (thicknesses in nm [5 Ta / 25 CuN]x6 / 5 Ta / 5 Ru / 6 IrMn / 2.0 CoFe30 / 0.7 Ru / 2.6 $CoFe_{40}B_{20}$ / MgO / 2.0 $CoFe_{40}B_{20}$ / 0.21 Ta / 7 NiFe / 10 Ta / 7 Ru. The MgO barrier was deposited with a wedge profile across the wafer. Probing is done through FL and BL contact nobe with proper rotation

Equivalent circuit: An equivalent circuit model is shown at the bottom, where each magnetic tunnel junction is represented as a nonlinear resistive element connected to the shared field line. This model is used to interpret the measured electrical and spectral responses.

1.2. Results

Figure S2 shows the field-line (FL) current sweep hysteresis measurements for MRAM devices 1 through 8 for a single array sample, measured at a constant MRAM bias current of 50 µA. For each device, three consecutive sweeps were performed to evaluate switching behavior, repeatability, and stability. Across MRAM 2-6, the devices exhibit clear and well-defined hysteresis loops in resistance versus FL current, characteristic of robust magnetic switching. The resistance states separate cleanly into high-resistance (antiparallel) and low-resistance (parallel) branches, with abrupt transitions at the switching currents. The close overlap of the three sweeps for each device indicates good cycle-to-cycle repeatability and minimal drift.

The switching currents are generally consistent across the array, with transitions occurring symmetrically in the positive and negative FL current directions (approximately within the ±100-150 mA range, depending on the device). This suggests good uniformity of the free layer coercivity and effective field coupling across the array. Minor variations in switching thresholds and resistance levels are observed from MRAM to MRAM, which can be attributed to expected device-to-device process variations. MRAM 1 shows a more gradual and asymmetric resistance evolution compared to the other devices, with less abrupt switching and a narrower resistance window. This behavior may indicate partial switching, increase thermal effects, or reduce magnetic stability relative to the other cells.

Overall, MRAM 2-6 demonstrate stable, repeatable hysteretic switching, well-separated resistance states, and consistent behavior over multiple sweeps, confirming good functional integrity of the single-array sample under the applied bias and FL current conditions. However, MRAM1, MRAM7 and MRAM8 show little distortion in hysteresis.

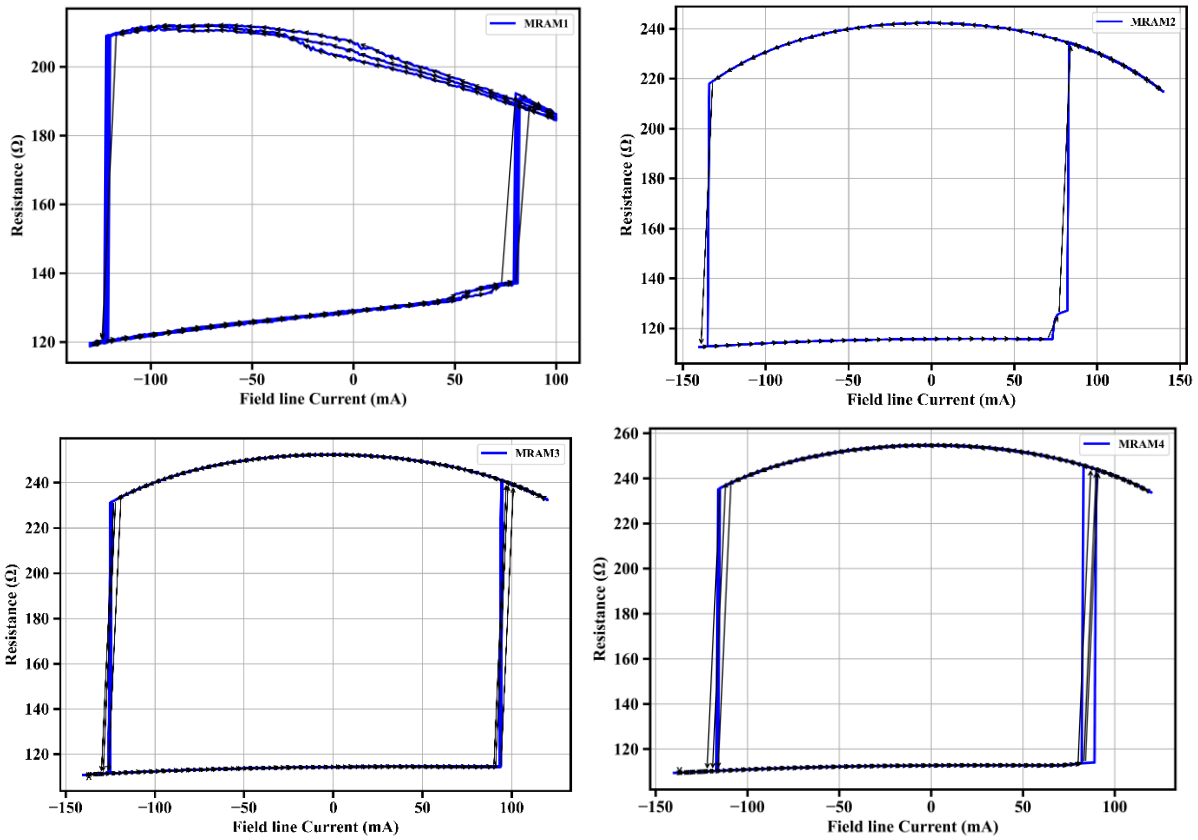

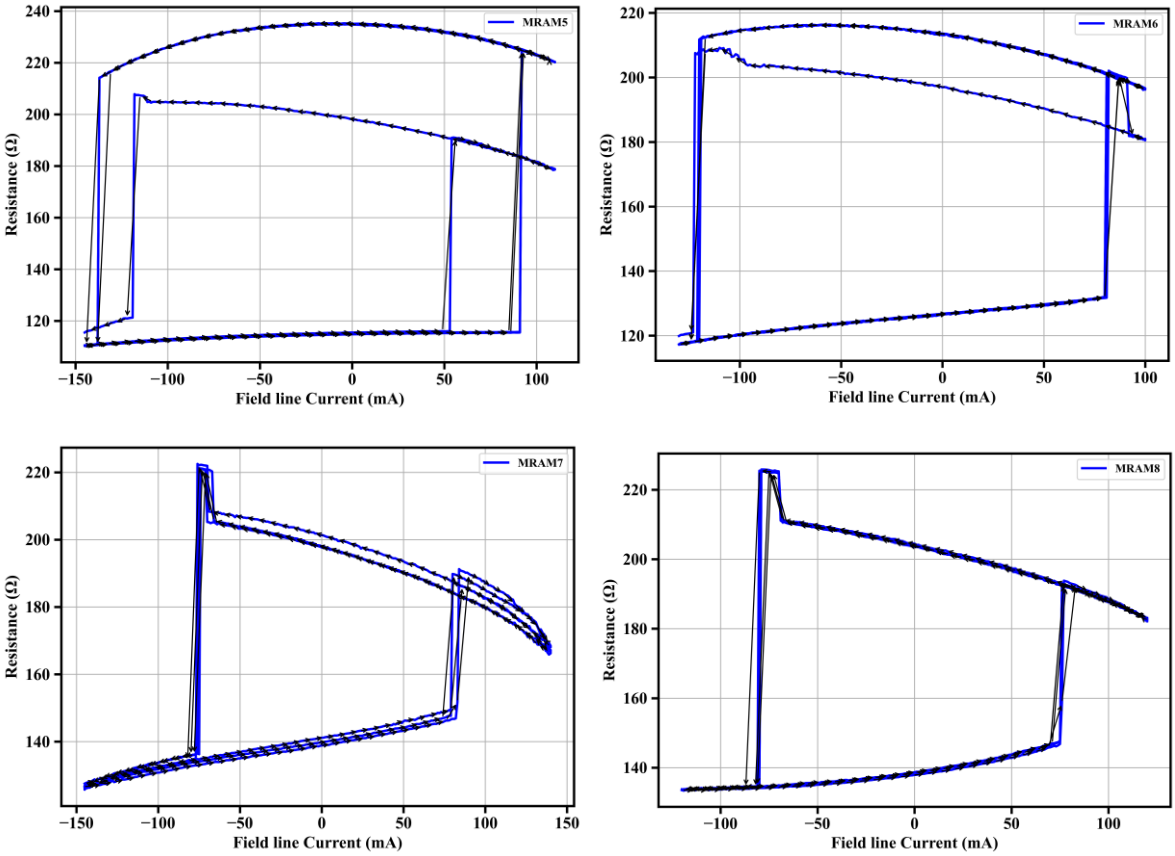

Figure S2. On-chip field-line (FL) current-induced hysteresis characteristics of MRAM cells 1-8 within a single array, measured at a constant MRAM bias current of 50 µA. The resistance of each cell is plotted as a function of FL current over three consecutive sweep cycles.

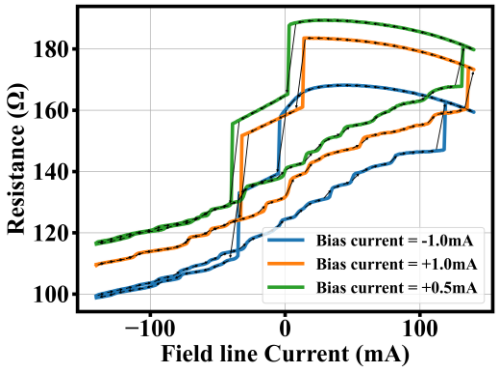

Figure S3: Field-line (FL) current sweep hysteresis of a spin-torque nano-oscillator **(STNO)** measured at a constant bias current of 50 µA with FL current swept from −0.14 A to +0.14 A. The device exhibits a multi-state, hysteretic response with an intermediate resistance region attributed to a vortex state

Figure S3 shows the field-line (FL) current sweep hysteresis of STNO measured on a single array at various bias current, with the FL current swept between −0.14 A and +0.14 A. The STNO exhibits a non-binary, multi-state resistance evolution with pronounced hysteresis, reflecting complex magnetization dynamics rather than abrupt two-state switching. At negative FL currents, the resistance increases gradually with current magnitude, indicating progressive magnetization rotation. A distinct intermediate resistance regime is observed around moderate negative currents, highlighted in the figure

and attributed to the formation of a vortex state. As the FL current approaches zero and reverses polarity, a sharp resistance transition occurs, signaling a field-driven reconfiguration of the magnetic state. At positive FL currents, the resistance reaches a higher level and then decreases gradually with increasing current, completing the hysteresis loop. The directional arrows indicate the sweeping direction and emphasize the path-dependent nature of the switching process. The close overlap among the three sweeps demonstrates good repeatability and stability of the STNO magnetic states under repeated FL current cycling. Overall, the measured hysteresis confirms the presence of vortex-mediated switching behavior and highlights the rich magnetic dynamics of the STNO under field-line excitation.

2. Device characterization with external field line

2.1. Characterization setup and methods

Figure S4 illustrates the Experimental characterization setup for measurements under an externally applied magnetic field. (a) - (b) Photograph of the device-under-test mounted inside a custom-designed copper toroidal coil used to generate a controllable external magnetic field. The magnetic field strength is tuned by adjusting the coil current supplied to the toroidal structure, allowing systematic investigation of magnetic-field-dependent switching and hysteresis behaviour of the MRAM devices. The probe assembly provides stable electrical contact to the chip during field application. (c) Schematic representation of the electrical biasing configuration and magnetic field distribution. The external field line is driven using an independent SMU to control the magnetic excitation current, while a separate bias line applies the MRAM read/write bias current. The schematic also illustrates the resulting magnetic field profile generated around the device region, highlighting the spatial distribution of the applied field and its interaction with the MRAM cell during characterization.

MRAM characterization: Two independent electrical paths are employed. The field line (FL) is driven by an SMU with a voltage compliance of $V_{\mathrm{lim}} = 3$ V and a current range of ± 1 A, generating a local magnetic field along the device through the on-chip field line. The bias line (BL) is driven by a second SMU with a voltage compliance of $V_{\mathrm{lim}} = 0.8$ V and a current range of ± 1 mA. The bias SMU is also used to measure the device resistance prior to each measurement to ensure reliable probe contact. An additional external magnetic field is applied using a copper toroidal coil positioned concentrically around the sample, as shown in Figure S4 (b). A controlled current through the toroid generates a predominantly circumferential magnetic field, with the resulting leakage flux providing a uniform in-

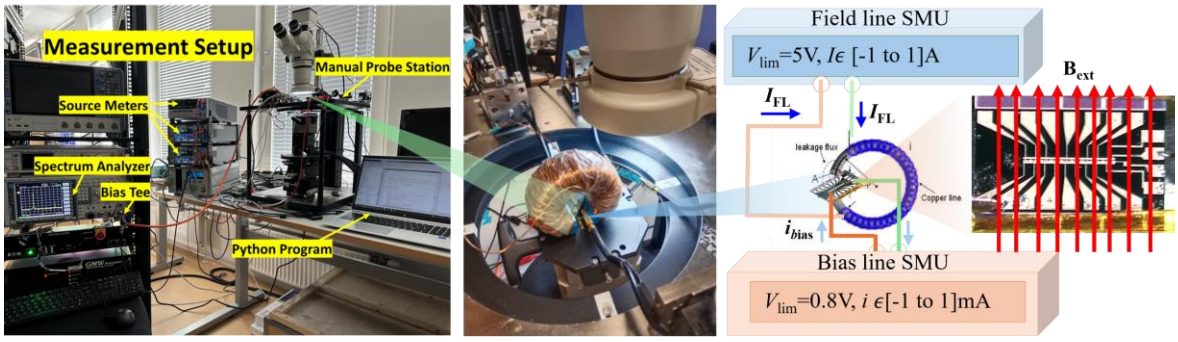

Figure S4: Experimental characterization setup with external magnetic field. (a) shows the measurement setup comprising a manual probe station, source-measure units (SMUs), bias-tee, spectrum analyzer, and a Python-controlled data acquisition system. (b) shows the sample positioned within a copper toroidal coil used to generate an external magnetic field via controlled coil current. (c) illustrates the electrical biasing scheme, where the external field line is driven by an SMU and the bias line is driven independently, along with a schematic of the resulting magnetic field distribution across the device.

plane magnetic field component at the device location. The magnitude and polarity of the external field are controlled by the coil current, enabling systematic field sweeps without mechanical realignment of the sample.

STNO characterization: For spin-torque nano-oscillator (STNO) measurements, a bias-tee is used to separate the DC bias current from the high-frequency voltage oscillations generated by the device. The DC component biases the device through the SMU, while the RF signal is routed to a spectrum analyzer. Measurement parameters such as frequency span, resolution bandwidth (RBW), and acquisition points are optimized to balance spectral resolution, noise floor, and measurement time.

- **Field line** (FL): Driven by an SMU with a voltage compliance of $V_{\text{lim}} = 5$ V and current range $I_{\text{FL}} \in [-1, +1]$ A. This line generates the magnetic field required for device switching.
- **Bias line** (BL): Driven by a separate SMU with a voltage compliance of $V_{\text{lim}} = 1$ V and current range $i_{\text{bias}} \in [-5, +5]$ mA, used to bias the magnetic tunnel junctions and reading the resistance state.

2.2. Results

Figure S5 presents the external field-line (FL) current sweep for external magnetic field generation for hysteresis measurements of MRAM cells 1 to 8 of a single array sample, characterized in the presence of an external magnetic field (applied using an external magnet, toroid). The FL current was swept between −1.0 A and +1.0 A, while the MRAM devices were biased at 50 μA. For each device, three consecutive sweeps were recorded to assess switching behavior, repeatability, and field-induced stability.

Most devices (MRAM 1-8) exhibit sharp, rectangular hysteresis loops with well-defined transitions between low-resistance (parallel) and high-resistance (antiparallel) states. The switching events occur abruptly at relatively high FL currents, reflecting the enhanced magnetic stability and increased switching thresholds resulting from the applied external magnetic field. The close overlap among the three sweeps for each cell demonstrates excellent cycle-to-cycle repeatability and minimal resistance drift. Device-to-device variations are observed in the exact switching current values and resistance levels, which are attributed to local magnetic field nonuniformity, lithographic variations, and differences in magnetic anisotropy across the array. MRAM 8, measured with an opposite sweeper polarity, confirms the reversible and symmetric switching behavior under reversed FL current direction in the presence of the external field. Overall, the measurements demonstrate that the application of an external magnetic field leads to robust, stable, and highly repeatable binary switching in most cells of the single array, while also highlighting isolated non-ideal behavior that provides insight into field–device interactions and array-level variability.

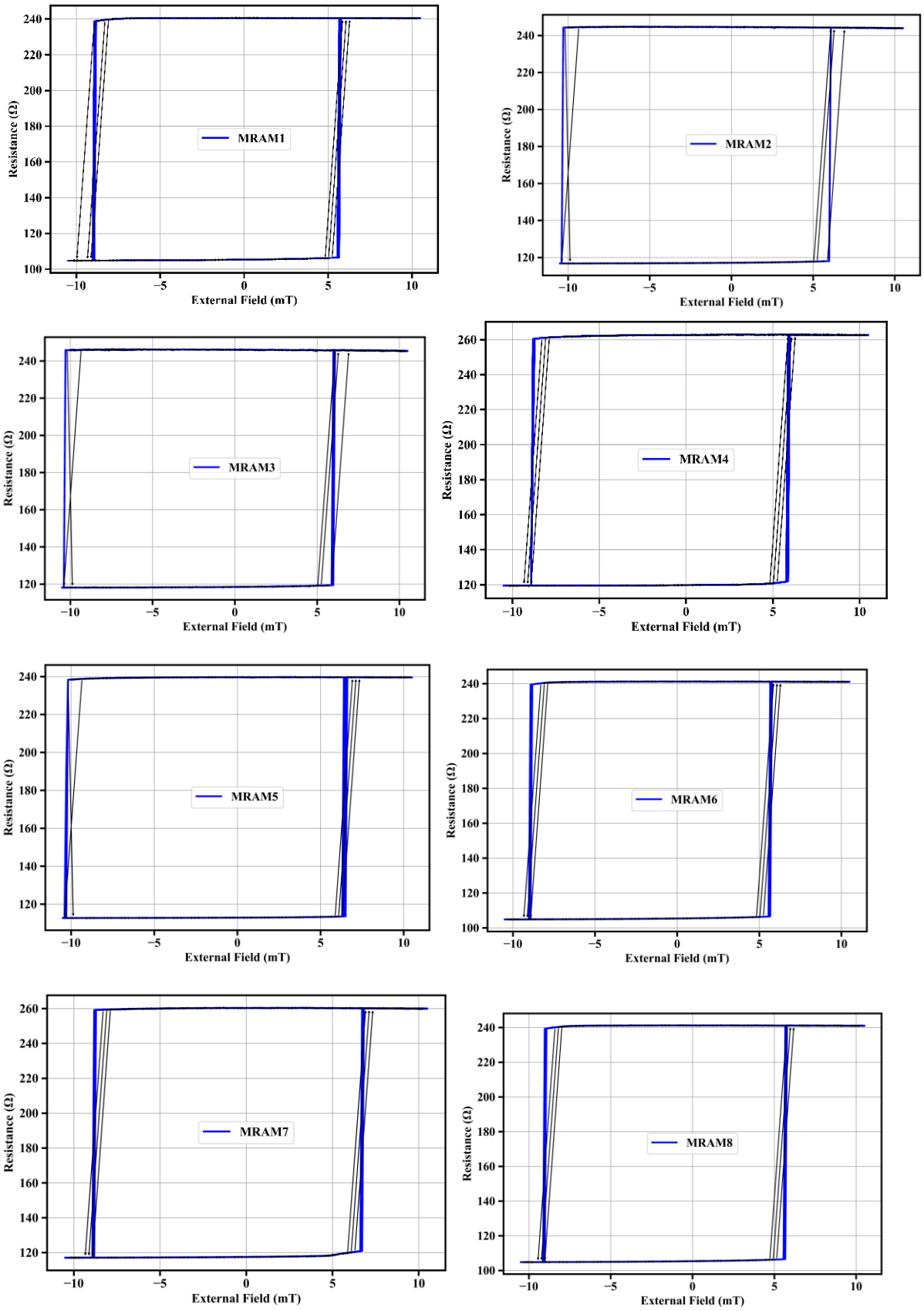

Figure S5: External field-line (FL) current-induced hysteresis characteristics of MRAM cells 1-8 from a single array measured in the presence of an external magnetic field. The FL current is swept from -1.0 A to +1.0 A while the MRAM devices are biased at 50 μA and resistance is plotted versus FL current for three consecutive sweeps.